Kinetics of Fibrinopeptide Release by Thrombin as a Function of $CaCl_2$ Concentration: Different Susceptibility of FPA and FPB and Evidence for a Fibrinogen Isoform-Specific Effect at Physiological Ca^{2+} Concentration†

Aldo Profumo,‡ Marco Turci,‡ Gianluca Damonte,§ Fabio Ferri,|| Davide Magatti,|| Barbara Cardinali,|| Carla Cuniberti,⊥ and Mattia Rocco*,‡

U.O. Biologia Strutturale, Istituto Nazionale per la Ricerca sul Cancro, Genova, Dipartimento di Medicina Sperimentale, Università di Genova, Genova, Dipartimento di Scienze CCFFMM and INFM, Università dell'Insubria a Como, Como, and Dipartimento di Chimica e Chimica Industriale, Università di Genova, Genova, Italy

Received March 17, 2003; Revised Manuscript Received August 18, 2003

ABSTRACT: The kinetics of release of fibrinopeptide A (FPA) and B (FPB) by thrombin were investigated on unfractionated fibrinogen samples as a function of $CaCl_2$ concentration. A 50 mM Tris, 104 mM NaCl, pH 7.4 (TBS) buffer, to which 1 mM EDTA-Na_2 (TBE) or 2.5 (TBC2.5), 14 (TBC14), and 30 mM $CaCl_2$ (TBC30) was alternatively added, was employed. The % FPA versus time curves were fitted with single stretched-exponential growth functions, where the stretch parameter β likely reflects substrate polydispersity ($\beta = 1$, monodisperse). For TBE, TBS, TBC14, and TBC30, we found $\beta \approx 1$, with corresponding normalized rate constants (K_a) of 3.8, 4.2, 2.7, and 1.9×10^{-5} [(NIHu/L)s]$^{-1}$. Surprisingly, in TBC2.5 we found $\beta = 0.69$, with an "average" K_a of 3.5×10^{-5} [(NIHu/L)s]$^{-1}$. This effect disappeared {$\beta = 0.97$, $K_a = 2.7 \times 10^{-5}$ [(NIHu/L)s]$^{-1}$} with an increase in the ionic strength I to that of TBC30 with 186 mM NaCl (TBCaNa buffer). FPB releases were instead consistent with a nonstretched consecutive exponential growth function, except in TBC30 where some FPB appeared to be cleaved independently. Log−log plots of K_a versus Ca^{2+} concentration, Cl^- concentration, or I showed a strong linear correlation with only the latter two except in TBCaNa, again suggesting specific effects of the physiological Ca^{2+} concentration and I on FPA release. The corresponding K_b plots showed instead that both total depletion and high Ca^{2+} hampered FPB release. To further investigate the TBC2.5 $\beta = 0.69$ effect, FG polydispersity was assessed by Western blot analyses. The thrombin-binding γ'-chain isoform was ∼4%, resulting in a bound:free thrombin ratio of ∼25:75. With regard to the C-terminal ends of the Aα-chains, ∼45% were either intact or lightly degraded, while the remaining ∼55% were more degraded. Fitting the % FPA release data in TBC2.5 with a sum of two exponentials resulted in a faster component and a slower component ($K_{a1}/K_{a2} \approx 6$), with a ratio of ∼48:52. While a role for the γ'-chain isoform cannot be excluded, this good correlation with the C-terminal degradation of the Aα-chains suggests their calcium-dependent involvement in FPA release.

Fibrinogen (FG)[1] is a high-molecular mass (340 000 Da), centrosymmetric, dimeric glycoprotein whose physiological blood concentration ranges from 3 to 4 mg/mL (∼10^{-5} M) (*1*, *2*). Each half consists of three polypeptide chains, termed Aα, Bβ, and γ, which in the human species contain 610, 461, and 411 amino acid residues, respectively (*2*−*4*). All six N-termini are contained in a central, globular domain ("E-domain"), joined by two coiled-coil connectors to two outer globular domains ("D-domains"), formed by the C-terminal parts of the Bβ- and γ-chains, as deducted from early biochemical and biophysical studies and recently confirmed by crystallography (*2*−*8*). The location of the ∼400 C-terminal amino acids of the Aα-chains is instead still controversial, ranging from partially free-swimming appendages to forming a fourth globular domain positioned on top of the central one (*8*−*13*). It should also be noted that alternative splicing of the Aα-chain and especially the γ-chain mRNA, post-translational modifications, and proteolytic cleavage mainly in the C-terminal parts of the Aα-chains combine to produce a great variety of circulating FG isoforms and partially degraded species, some of which have defined physiological roles (reviewed in refs *14* and *15*).

† Partially supported by grants from the Italian Space Agency (ASI) to M.R. and F.F.

* To whom correspondence should be addressed: Medicina Rigenerativa, IST c/o CBA, Largo R. Benzi 10, I-16132 Genova, Italy. Telephone: +39-0105737-310. Fax: +39-0105737-325. E-mail: rocco@cba.unige.it.

‡ Istituto Nazionale per la Ricerca sul Cancro.

§ Dipartimento di Medicina Sperimentale, Università di Genova.

|| Università dell'Insubria a Como.

⊥ Dipartimento di Chimica e Chimica Industriale, Università di Genova.

[1] Abbreviations: FG, fibrinogen; FPA, fibrinopeptide A; FPB, fibrinopeptide B; FP(s), fibrinopeptide(s); Tris, tris(hydroxymethyl)-aminomethane; PAA, polyacrylamide; DTT, dithiothreitol; TBS, 50 mM Tris, 104 mM NaCl, pH 7.4 buffer; TBE, TBS with 1 mM EDTA-Na_2; TBC2.5, TBS with 2.5 mM $CaCl_2$; TBC14, TBS with 14 mM $CaCl_2$; TBC30, TBS with 30 mM $CaCl_2$; TBCaNa, 50 mM Tris, 186 mM NaCl, 2.5 mM $CaCl_2$, pH 7.4 buffer.

10.1021/bi034411e CCC: $25.00
Published on Web 09/30/2003

The N-termini of FG Aα- and Bβ-chains each contain a cryptic polymerization site masked by short amino acid sequences, called fibrinopeptide A (FPA) and fibrinopeptide B (FPB), that can be enzymatically removed. This event generates a reactive species, monomeric fibrin, that rapidly polymerizes mainly by interaction of the newly exposed knob-like N-terminal sequences (*A* and *B* sites) with "holes" always present in the γ- and Bβ-chains (*a* and *b* sites), respectively, in the outer domains, producing in the early stages two-stranded, half-staggered "protofibrils" which then aggregate laterally, ultimately forming a network of fibers known as the fibrin clot (see refs *2* and *3*, and references therein). In humans, the physiological release of FPA and FPB is due to the cleavage of the Aα Arg16−Gly17 and Bβ Arg14−Gly15 bonds, respectively, promoted by thrombin, a trypsin-like enzyme with a much narrower substrate specificity (*2*, *3*, *16*). In the early stages of the reaction, FPA is released at a considerably higher rate than FPB so that, by the time a visible clot appears, little FPB has been cleaved under physiological or quasi-physiological conditions (see Figure 5 of ref *2*, and references therein). The FPA-less, partially activated fibrin monomer species is often termed desAA-fibrin, and the release of FPB from desAA-fibrin generates desAABB-fibrin. The relationship between the cleavage of the two sets of fibrinopeptides (FPs) and the sequential events in the fibrin gel formation has been puzzling for a long time (see refs *2* and *3*). Apparently, the onset of gelation greatly enhances the release of FPB from the desAA-fibrin (proto)fibrils so that the extent of lateral aggregation grows at an exponential rate thereafter (*2*, *17*). Studies with other enzymes (mainly from snake venoms), which selectively release only one pair of FPs or the other, have shown that removal of either the FPAs or the FPBs is sufficient to trigger the formation of the two-stranded protofibrils and their subsequent lateral aggregation, although the desBB-fibrin gels form only at lower than physiological temperatures (see ref *18*, and references therein). However, the removal of FPBs seems to enhance the formation of thicker fiber bundles (*18*). The recent modeling work by Doolittle and collaborators (*19*) has advanced an explanation for these observations, showing how the *B*−*b* engagement, besides allowing protofibril formation *per se*, could also lead to better exposure of a reactive patch favoring their lateral aggregation. It must be also pointed out that the mechanism of FP release by the physiological enzyme thrombin and that of the more selective venom enzymes could be very different, and thus greatly influence the kinetics of fibrin assembly (see refs *20* and *21*, and references therein). For instance, it appears that thrombin can release the second FPA faster than the first from a single FG molecule, although the estimates of the magnitude of this effect vary between a factor of 3 and 16 (*22*−*24*), while the snake venom enzyme ancrod seems to cleave both FPAs independently (*25*, *26*).

The fibrinogen−fibrin transition and FP release have also been extensively studied for their involvement in other pathophysiological processes such as angiogenesis and metastatic spread (*27*, *28*). An increased rate of FPA release has been associated with various malignancies (*29*). A better response to chemotherapy has been observed in patients with low levels of FPA than in those with higher levels; furthermore, normal levels of FPA have been found in patients in prolonged complete remission (*30*). As a consequence of these results, the evaluation of FPA release has been recently proposed to be a prognostic factor in patients with malignant diseases (*31*).

Calcium ions are important cofactors in the blood coagulation system. However, the precise number, affinity, and location of FG Ca^{2+}-binding sites are not fully resolved issues. Early work by Nieuwenhuizen, Haverkate, and colleagues (see refs *32*−*35*, and references therein) seemed to indicate a difference between rat and human fibrinogen, the former having approximately three high-affinity and two low-affinity sites, and the latter lacking the low-affinity ones. Previously, three high-affinity and several low-affinity sites were instead reported by Marguerie and colleagues for bovine FG (*36*). Two of the three high-affinity sites were readily localized in the outer D domains (*32*−*35*), and subsequently identified by crystallography near the *a* polymerization hole in the C-terminal portion of the γ-chain (*5*, *6*). Surprisingly, in another crystal structure consisting of a cross-linked human D dimer with two synthetic short analogues of the *A* and *B* knobs bound, a second Ca^{2+}-binding site was found in a comparable position near the *b* polymerization hole in the C-terminal portion of the Bβ-chain (*37*). However, the lack of a fourth coordinating side chain, with respect to the γ-chain site, suggests that this may be one of the controversial lower-affinity Ca^{2+}-binding sites (*37*). Two more weak Ca^{2+}-binding sites were subsequently identified by the same authors (*38*) in human D dimers, although only one was evident in a recombinant human fragment D crystal structure (*39*). In addition, sialic acid residues have also been proposed to be low-affinity Ca^{2+}-binding sites (*40*). As for the elusive third high-affinity site, it has been suggested that it may be a composite site involving the C-terminal ends of both Aα-chains (*35*, *41*, *42*). In any case, it is known that Ca^{2+} ions play a role in the stabilization of fibrinogen against heat denaturation and plasmin digestion (*3*, *41*, *43*), and it has been observed that the removal of calcium induces conformational and functional changes (*44*). The presence of several low-affinity binding sites for calcium is supposed to influence the fibrin polymer distribution in the growing network (*2*, *40*, *45*). In the course of an extensive study on calcium ions binding to fibrin during clot formation, Mihalyi showed that there is an uptake of Ca^{2+} that runs parallel to FPB release, while FPA is released largely during its lag period (*46*). Overall, calcium ions are known to accelerate the fibrinogen−fibrin transition promoted by thrombin, decreasing the clotting time (*2*, *45*).

FP release kinetics have been studied carefully in the past, and values of k_{cat} and K_M have been reported for both FPA and FPB cleavage (*47*−*51*). However, bovine and human proteins were employed in various combinations, and buffer conditions and temperature were very different from study to study. Moreover, notwithstanding its prominent role in the blood coagulation system, the effect of the Ca^{2+} concentration was not systematically studied, to the best of our knowledge.

We present here an investigation of the kinetics of FP release from human FG by human thrombin as a function of Ca^{2+} concentration, in a buffer with an ionic strength and a pH that are close to physiological values. To relate these values to our ongoing studies of fibrin formation (*21*, *52*−*54*), we performed the assays at room temperature (25 ± 2

°C), and at a single, relatively low FG concentration (0.5 mg/mL). The data were fitted to appropriate equations derived from various enzymatic schemes. The dependence of the normalized rate constants K_a and K_b on the different ions present in solution or on the total ionic strength I was analyzed as proposed by Vindigni and Di Cera (*51*), revealing a different susceptibility of the two sets of FPs. In addition, a noticeable effect of physiological Ca^{2+} concentration was observed at physiological ionic strength on the FPA release only, suggesting the presence of at least two subpopulations with different release kinetics. A possible correlation to the inherent polydispersity of our FG samples was attempted, and the implications of these findings for FG structure−function relationship, and for the process of fibrin formation, are discussed.

MATERIALS AND METHODS

Materials. All reagent grade chemicals were purchased from Merck (Darmstadt, Germany), unless otherwise stated. Doubly distilled water was always employed in the preparation of the solutions. Blood samples were obtained from two healthy donors (A.P. and M.R.) in K_3EDTA-containing tubes, and centrifuged at 4 °C initially for 10 min at 500*g*, and then for 15 min at 2000*g* to separate the plasma from the cellular components. Samples for electrophoresis (see below) were then immediately prepared from the plasma fractions assuming a physiological FG concentration of 3 mg/mL.

Fibrinogen Preparation and Quality Control. Lyophilized human FG (TF grade, lot 05, IMCO, Stockholm, Sweden) was dissolved at 37 °C at a nominal concentration of 20 mg/mL in 0.3 M NaCl, to which 10 units/mL KIR (serine protease inhibitor, Richter, Milan, Italy) was added; it was then dialyzed twice at 4 °C for 4 h against TBS buffer [50 mM tris(hydroxymethyl)aminomethane (Tris) and 104 mM NaCl (pH 7.4)]. A specific absorption coefficient E of 1.51 mL mg^{-1} cm^{-1} was employed to determine the FG concentration from the absorbance at 280 nm (*55*), after correcting for scattering contributions by subtracting the absorbance at 320 nm. All spectroscopic measurements were performed in a Beckman DU-640 spectrophotometer (Beckman Analytical, Milan, Italy). FG was tested for purity, and plasma samples were analyzed, by means of polyacrylamide (PAA) gel electrophoresis in the presence of sodium dodecyl sulfate (SDS−PAGE) of samples reduced with dithiothreitol (DTT, Sigma-Aldrich, Milan, Italy) according to the method of Laemmli (*56*); electrophoresis grade reagents from Bio-Rad (Hercules, CA) were used. A careful characterization of commercial purified and plasma FG subpopulations was performed by means of wet Western blotting, utilizing 0.45 μm pore size nitrocellulose membranes (Hybond-C, Amersham Pharmacia Biotech, Uppsala, Sweden), in a similar way as we have previously reported (*21*). The IgM Y18 monoclonal antibody (MAb) (a generous gift of W. Nieuwenhuizen, Leiden, The Netherlands), directed against an epitope on the FPA (*57*), was employed to recognize the Aα-chains, followed by color development using a horseradish peroxidase-conjugated goat anti-mouse IgM secondary antibody (Southern Biotechnology Associates, Birmingham, AL) and 4-chloro-1-naphthol (Fluka Chemie, Buchs, Switzerland) as a substrate. For FG, each sample was run in duplicate, and half of the blot was instead stained with amido black (Sigma). Prestained recombinant protein molecular mass markers (250−10 kDa, Bio-Rad catalog no. 161-0372) were also run on the gels and likewise blotted. Plasma samples were instead run side by side with commercial FG samples and immunostained only. The blots were then scanned on a Mustek MFS 6000CX flatbed scanner using a 600 × 600 dpi resolution, and the optical density (OD) profile for each lane was determined with the One-Dscan software (Scanalytics, CSPI, Billerica, MA) followed by Gaussian deconvolution of overlapping peaks using PeakFit version 4 (Jandel Scientific, now distributed by Systat Software Inc., Richmond, CA). Likewise, the relative content of normal γ-chains and of its longer γ' splice variant (*58*) was determined on FG blots using the IgG1 mouse MAbs 4A5, directed against an epitope present in residues γ392−411 (*59*) (kindly provided by G. Matsueda, Bristol-Myers Squibb), L2B, specific for the γ'-chain extension, and J88B, which recognizes all γ-chain forms (*60*, *61*) (L2B and J88B were both a generous gift of P. J. Simpson-Haidaris, University of Rochester, Rochester, NY), and a goat anti-mouse IgG1 horseradish peroxidase-conjugated secondary antibody (Southern Biotechnology Associates).

Thrombin Preparation and Titration. Lyophilized human thrombin was from Sigma (catalog no. T-6884, lot 20K7614, nominal activity of 2330 NIH units/mg of protein). It was reconstituted with exactly 1 mL of water (measured with a Hamilton syringe and checked by weight) to a final nominal concentration of 1199 NIH units/mL, and stored in small aliquots at −80 °C until it was used. To normalize to the same thrombin concentration data sets obtained from experiments performed months apart, the enzymatic activity of the employed thrombin solution was measured, immediately after reconstitution and prior to each experiment, with the chromogenic substrate *N*-benzoyl-Phe-Val-Arg-*p*-nitroanilide (Sigma B-7632). Assuming that the total loss of enzymatic activity over time was due to degradation of α- and β-thrombins to the same extent, we then normalized each experiment to the initial content of NIH units. The thrombin assay was performed using the method of Lottenberg et al. (*62*).

Fibrinopeptide Release. Briefly, triplicate 1.5 mL solutions containing 0.5 mg/mL FG were incubated with thrombin at 0.25 nominal NIH unit/mg of FG in Eppendorf microcentrifuge tubes for different times (1, 2, 5, 10, 15, 30, 60, and, if required, 120 min) at room temperature, after which the tubes were rapidly placed into and kept for 1 min in boiling water. After centrifugation at 16000*g* for 15 min, the supernatant was filtered through 25 mm diameter, 0.45 μm pore size polyethersulfone syringe filters (Millex-GP, Millipore, Bedford, MA). The samples were then stored at 4 °C until they were analyzed. The temperature of the room was stable within ±0.5 °C during each experiment, but it could differ from experiment to experiment because of seasonal variations (25 ± 2 °C). The buffers that were used were based on TBS, to which 1 mM EDTA-Na_2 (TBE) or 2.5 (TBC2.5), 14 (TBC14), or 30 mM $CaCl_2$ (TBC30) was alternatively added. In addition, a 50 mM Tris, 186 mM NaCl, 2.5 mM $CaCl_2$, pH 7.4 (TBCaNa) buffer, having the ionic strength of TBC30 and the Ca^{2+} content of TBC2.5, was also employed.

Determination of the Effective End Point of the Reactions. After being immersed in boiling water, the samples take some

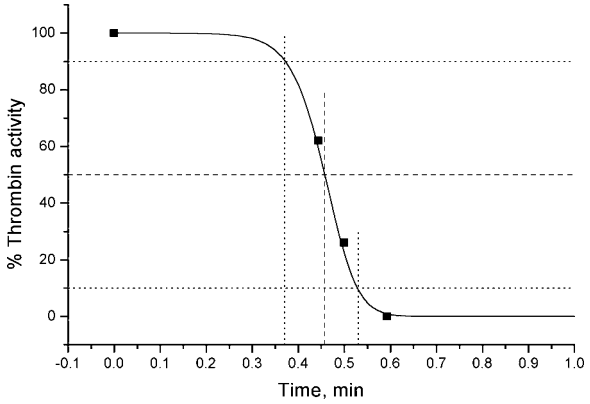

FIGURE 1: Determination of the effective end point of the reaction: % thrombin activity (■) vs time *t* elapsed after immersion in the boiling water. The solid curve represents the best fit to the data according to eq 1.

time to reach the temperature at which thrombin becomes inactive. The rate at which the sample temperature increases with time was determined by using a small thermistor probe inserted in an Eppendorf microcentrifuge tube filled with buffer only.

The dependence of thrombin activity on temperature was determined, using the same *p*-nitroanilide substrate as described above, by measuring the enzymatic activity at 45, 50, and 55 °C, which was found to be 62, 26, and 0%, respectively, of that measured at 25 °C. The tests were done by rapidly adding a small volume of enzyme kept at room temperature to the solutions contained in cuvettes already pre-equilibrated at the requested temperature. No appreciable degradation of the substrate was observed at these temperatures, as determined by performing the kinetic analyses at 25 °C on samples that had been kept for ~3 h at the higher temperature. A further check was subsequently done by measuring the FP release after adding a relatively small volume of a thrombin solution kept at room temperature to FG solutions kept at 50 or 55 °C in the same Eppendorf tubes used for all the experiments, placed in a thermostated water bath. For comparison, FP releases were also assessed in parallel on samples kept at room temperature. The reactions were stopped after 1 or 5 min, and FP release was analyzed via HPLC as described below. A small percentage of residual activity remained, but it proportionally decreased with the incubation time, leading to a substantial agreement with the synthetic substrate data.

Via combination of the information about how the sample temperature increases with time and how the thrombin residual activity decreases as a function of temperature, it is possible to determine how the thrombin activity deteriorates with time after placing the tubes in the boiling water bath. This is shown in Figure 1, in which the filled squares correspond to the thrombin inactivation data, while the solid curve represents their corresponding interpolating curve, based on the empirical equation:

$$\alpha(t) = 100(1 + ae^{\delta}t)^{-\nu} \qquad (1)$$

where $\alpha(t)$ is the percent thrombin activity as a function of time t (minutes) after immersion in the boiling water and a, δ, and ν are adjustable parameters, whose best values were found to be 8×10^{-6}, 24 min^{-1}, and 1.8, respectively.

As can be seen in Figure 1, the transition from full to zero activity is quite sharp and occurs at 0.457 min, as determined by evaluating the time at which the activity is reduced to 50% (dashed lines). The width of the transition, estimated between 90 and 10% of its initial value (dotted lines), was 0.06 min. In conclusion, the effective time at which the reaction is "instantaneously" stopped was estimated by adding the lag time (Δt) of 0.46 ± 0.06 min to the time at which the sample is immersed in the boiling water.

Separation of Fibrinopeptides. FPs were separated by reverse-phase high-pressure liquid chromatography (RP-HPLC) on a Beckman System Gold composed of a 126 Solvent Module and a 166 UV/VIS Concentration Detector, with slight modifications of the method of Kehl et al. (*63*). Using the filled loop method, exactly 1 mL of the sample was loaded on a 4.6 mm × 250 mm column preceded by a 4.6 mm × 45 mm guard column (both Ultrasphere ODS, 5 μm particle diameter, Beckman). The system was equilibrated in 88% NH_4CH_3COO (25 mM), brought to pH 6 with diluted H_3PO_4 (buffer A), and 12% NH_4CH_3COO (50 mM), brought to pH 6 with H_3PO_4 and then diluted 1:1 with CH_3CN (buffer B). NH_4CH_3COO was from Fluka Chemie, and CH_3CN was LiChroSolv from Merck. The flow rate was 1.5 mL/min, and elution was performed with this sequence: isocratic 88% A and 12% B for 5 min and then a linear gradient over the course of 40 min to 72% A and 28% B. The elution was monitored at 211 nm, and the FPs eluted in the order reported by Kehl et al. (*63*). Entrapment of FPB in the clot (*51*) was found to be negligible, after dissolution of a sample in 8 M urea and analysis via RP-HPLC.

Identification of Fibrinopeptides. An electrospray mass spectrometry (ESPI-MS) analysis was performed to characterize the HPLC peaks. All the chromatographic conditions were the same as described above, but the concentration of the injected material was 10 times higher. The direct coupling of the HPLC system (HP 1090, Hewlett-Packard, Palo Alto, CA) with an HP MS-Engine mass spectrometer equipped with an atmospheric pressure ionization source allowed the identification of all the separated peaks by the comparison of the measured molecular masses with the expected ones. Mass spectra, ranging from 500 to 1900 *m*/*z*, were acquired in the positive ion mode using an HP 5989A single quadrupole, and the capillary exit voltage was set to 215 V. All the peptide masses were calculated by deconvoluting the measured *m*/*z* ratio of at least two multicharged ions.

Quantification of Fibrinopeptides. The amount of FPs was determined from the area of each peak. Data collection was done by the System Gold Beckman software. Postrun data analysis was performed using PeakFit. No attempt was made to calibrate the system with known amounts of FPs because we were interested only in their relative amounts. The variants and degradation products of the two FPs (*63*) eluting as single peaks or shoulders were grouped together with those of the intact ones as total FPA and total FPB.

Curve Fitting. The % FP release versus time data were fitted using a nonlinear least-squares Levenberg−Marquardt algorithm implemented in a Lab-View 6.1 environment (National Instruments, Austin, TX). The error associated with the *x* variable (time) was projected on the *y* variable (% FP release) using standard methods (*64*). The equations that were

employed were derived from those of Mihalyi (*50*). For FPA, a modified single-exponential growth equation, including a stretch exponent β_a, was used:

$$\mathrm{FPA} = A[1 - e^{-(k_a t)^{\beta_a}}] \quad (2)$$

in which A is the amplitude, k_a the rate constant for FPA release, and t the time. The amplitude A was constrained to 100 ± 1.5, to reflect the uncertainty associated with the final plateau determination. The stretch parameter β_a was introduced to check for dispersive nonexponential kinetics. If $\beta_a = 1$, the process exhibits genuine first-order kinetics, characterized by a unique time-independent rate constant k_a and by a single-exponential decay function. When $\beta_a < 1$, either the rate constant k_a is time-dependent, with its value decreasing with time, or there is a distribution of time-independent rate constants, reflecting a inhomogeneous distribution or a polydispersity of the reactant species (for instance, see refs *65* and *66*, and references therein). Both mechanisms may lead to the same relaxation behavior, and there is no way to distinguish between them, unless the kinetic data are complemented with other types of measurements or analysis. For this reason, we have attempted a correlation of our kinetic data with the polydispersity analysis carried out on the FG samples as described above. Therefore, in one single case, the kinetic data were also fitted to a sum of two single exponentials given by

$$\mathrm{FPA} = A_1(1 - e^{-k_{a1}t}) + A_2(1 - e^{-k_{a2}t}) \quad (3)$$

imposing the constraint $A_1 + A_2 = 100 \pm 1.5$.

With regard to FPB release kinetics, two models were considered. One of them assumes a consecutive reaction mechanism, in which FPB can be released only after FPA cleavage

$$\mathrm{FPB} = A\left[1 - \frac{k_b}{k_b - k_a}e^{-k_a t} + \frac{k_a}{k_b - k_a}e^{-(k_b t)^{\beta_b}}\right] \quad (4)$$

where k_b is the rate constant for the release of FPB from desAA-fibrin. The β_b stretch factor was inserted to determine if it would also lead to better fits, as in the case of FPA.

The second one contemplates also the direct release of FPB from native fibrinogen, although with a slower rate constant k_b':

$$\mathrm{FPB} = A\left[1 + \frac{k_b - k_b'}{k_a - k_b + k_b'}e^{-(k_a + k_b')t} - \frac{k_a}{k_a - k_b + k_b'}e^{-k_b t}\right] \quad (5)$$

Both eqs 4 and 5 were used only when the k_a values were obtained from eq 2 with a β_a of 1. When β_a seriously deviates from unity, it is not possible to use eq 4 or 5 directly. In this case, we solved numerically (Runge−Kutta method) the rate equation describing the release of FPB by imposing for FPA a release behavior given by eq 2. This procedure leads to a fitting function that is defined numerically, in which the only floating parameters are the amplitude A and the rate constant k_b (and k_b', if required), while k_a and β_a are kept fixed to the values previously found by fitting the FPA data with eq 2.

RESULTS

Kinetics of FP Release. Representative chromatographic separations of the fibrinopeptides at some selected times for a reaction in TBCaNa are shown in Figure 2, where the overall good quality of the separations can be appreciated. The FP peaks are identified on the background chromatogram, using the conventions of Kehl et al. (*63*). The peak labeled as unknown was proven not to be desArg-B by mass spectrometry. The complete series of experimental data points (each one being the average of three different runs) obtained after integration of the FP chromatographic peaks are reported in Figure 3 on lin−log graphs for the different buffers that were employed. For each experiment, the end point of the reaction was identified (usually 60 min, 120 min for TBC30), and the corresponding areas were taken to be 100% release. As can be seen in Figure 3, the standard deviations associated with the data are reasonably small, allowing us to perform a careful curve fitting analysis. Superimposed on the data in Figure 3 are the various curves that were obtained using the methods described in the previous section.

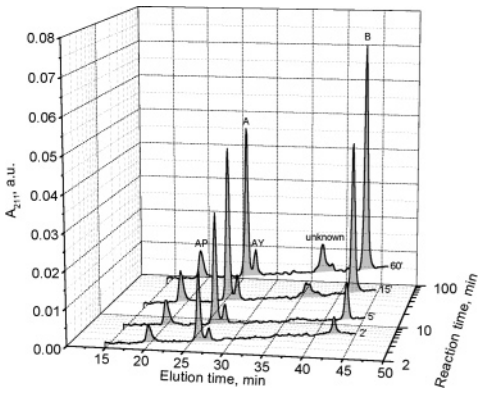

FIGURE 2: Representative RP-HPLC separations of FPs as a function of the reaction time. Four chromatograms of reactions stopped 2, 5, 15, and 60 min after addition of thrombin in TBCaNa buffer are shown. A log scale is used for the reaction time coordinates to allow for a better separation of the chromatograms in the graph.

To start, the FPA release curves were fitted with eq 2, fixing the stretch term to $\beta_a = 1$. This resulted in very good fits (Figure 3, filled squares and solid lines) in all cases except for buffer TBC2.5 (panel C). When β_a was allowed to vary, curves practically superimposable with those with a β_a of 1 were obtained in all cases except for TBC2.5, where the new curve, with a β_a of 0.69, instead fitted the data points very well (Figure 3, filled squares and dashed lines). It should also be pointed out that the fact that almost all the curves were accurately fitted when β_a was fixed to 1 is a consequence of the correction we have made to the time points to allow for the delayed thrombin inactivation (see Materials and Methods). In fact, removing this correction required a β_a of <1 for nearly all the curves, although it was confined to $\sim$0.9 in most cases, except for TBC2.5 for which it was <0.6.

The k_a values derived from the FPA fittings with eq 2 ($\beta_a = 1$) were inserted in eq 4 and in eq 5, and the FPB release data reported in Figure 3 (empty squares) were then fitted, except those collected in TBC2.5. As can be seen, the curves obtained with eq 4 (solid lines) are nearly superimposable with those obtained with eq 5 (dashed lines). Only in TBC30 (panel E) was an appreciably better fit obtained with eq 5. Moreover, no stretch factor was required to optimize the quality of the fits (e.g., $\beta_b = 1$ in eq 4). Since $\beta_a = 0.69$ in

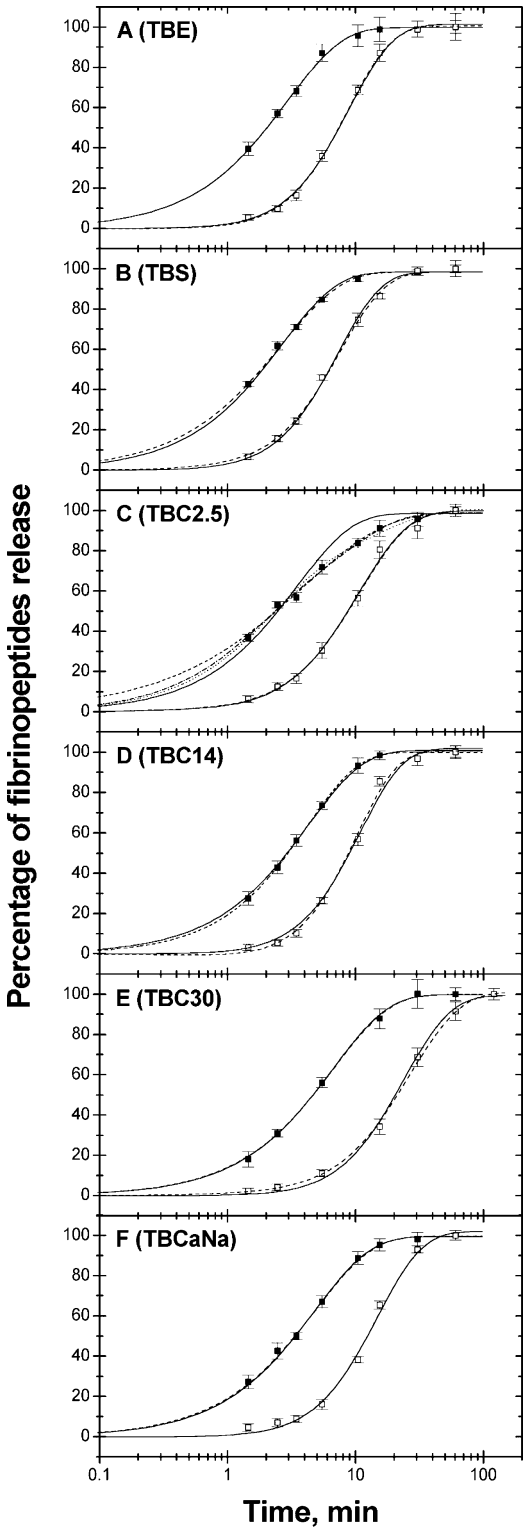

FIGURE 3: Lin−log plots of the percentage of FPA (■) and FPB (□) release vs time and relative curve fitting, as a function of $CaCl_2$ concentration. Superimposed are the results of fitting with eq 2 (FPA data; solid lines, $\beta_a = 1$; dashed lines, $\beta_a \neq 1$), with eq 3 (FPA data, panel C only; dotted line, 75:25 A_1:A_2; dashed and dotted line, 45:55 A_1:A_2), and with eqs 4 and 5 (FPB data; solid lines, eq 4; dashed lines, eq 5).

buffer TBC2.5, a different procedure had to be utilized to fit the corresponding FPB data with the equivalent of eqs 4 and 5, as outlined in Materials and Methods. The resulting curves are reported in Figure 3C, and they are again practically superimposable.

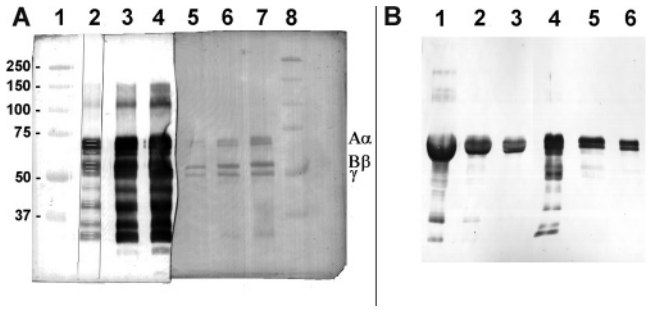

FIGURE 4: SDS−PAGE followed by Western blot analysis of reduced fibrinogen samples. Gels (8 cm × 10 cm, 0.75 mm thick), with a 1 cm 3% PAA stacking zone and a 5 cm 8% PAA resolving zone, were utilized. In panel A, lanes 1 and 8 contained prestained recombinant protein standards, with their molecular masses (kilodaltons) indicated on the left side and lanes 2−7 contained FG samples at different loading concentrations (lanes 2 and 5, 0.5 μg; lanes 3 and 6, 1.25 μg; lanes 4 and 7, 2.5 μg). The left half of the blot (lanes 1−4) was immunostained with the Y18 MAb, while the right half (lanes 5−8) was stained with amido black. Lane 2 was utilized for the densitometric analysis, with the two thin vertical lines defining the lane boundaries. (B) Lanes 1−3 contained plasma samples with nominal 0.5, 0.2, and 0.1 μg of FG loaded, respectively; lanes 4−6 contained 0.5, 0.2, and 0.1 μg of purified FG from Calbiochem, respectively. Immunostaining was carried out with the Y18 MAb.

The full set of kinetic constants deduced from the fits, normalized to 1 nominal NIH unit/L of thrombin (K_a and K_b), and the associated fit parameters are collected in Tables 1 and 2 for FPA and FPB, respectively, as a function of buffer conditions. The Ca^{2+}, Cl^-, and Na^+ molarities and the total ionic strength are also reported for each sample. For FPA, equal or very similar K_a values obtained for a β_a of 1 or when β_a was left to float (Table 1) are evident for all the buffers that were employed except for TBC2.5. In this case, a β_a of 0.69 leads to an approximately −12% change in the K_a value while clearly improving the quality of the fit, as indicated by the respective % rmsd values. As for the FPB release, the K_b values obtained using eq 4 ($\beta_b = 1$) or eq 5 are very similar in all cases except in TBS and TBC30, where it appears that some FPB may be released independently and not sequentially (Table 2). However, only for TBC30 is there also a marked (∼15-fold) improvement in the % rmsd on using eq 5. In any case, the effect is rather minor, with K_b' values being 1 order of magnitude smaller.

Estimating the Polydispersity of FG. To further investigate the reasons behind the $\beta_a = 0.69$ stretch factor in TBC2.5, we have examined the polydispersity of our FG samples. The major source of polydispersity is in the C-terminal portions of the Aα-chains, which are for instance highly susceptible to plasmin attack (*67*−*70*), although this enzyme does not seem to be the one responsible for the circulating lower-molecular mass FG forms (*71*). In Figure 4A, a Western blot of a PAA gel is shown, which was half-stained with amido black (right side), while the other half was immunostained with the Y18 MAb specific for a determinant in the FPA (left side). The two outer lanes (lanes 1 and 8) were loaded with prestained molecular mass markers, and the others were loaded with DTT-reduced FG samples at different loading concentrations. The amido black-stained FG samples (lanes 5−7) show the usual fibrinogen bands (indicated on the right side), with the doublet of the Aα-chains already pointing to the presence of heterogeneity.

Table 1: Kinetic Constants, Normalized to 1 NIH Unit of Thrombin/L, and Other Fitting Parameters (eq 2) for the Release of FPA as a Function of Ca^{2+} Concentration[a]

buffer	K_a {$\times 10^5$ [(NIHu/L)s]$^{-1}$}	β_a	A	% rmsd[b]	[Ca^{2+}] (mM)	[Cl^-] (mM)	[Na^+] (mM)	I (mM)
TBE	3.82 ± 0.08	1 (fixed)	99.8 ± 0.9	1.24	0	145	106	150
TBE	3.82 ± 0.09	1.00 ± 0.05	99.8 ± 1.0	1.25	0	145	106	150
TBS	4.20 ± 0.12	1 (fixed)	98.5 ± 0.9	1.80	0	145	104	145
TBS	4.20 ± 0.08	0.93 ± 0.02	98.5 ± 0.7	1.04	0	145	104	145
TBC2.5	3.95 ± 1.41	1 (fixed)	98.5 ± 3.8	7.58	2.5	150	104	153
TBC2.5	3.48 ± 0.30	0.69 ± 0.05	98.9 ± 2.4	3.90	2.5	150	104	153
TBC14	2.70 ± 0.05	1 (fixed)	101.0 ± 0.7	2.19	14	173	104	187
TBC14	2.77 ± 0.01	1.08 ± 0.01	100.0 ± 0.2	0.39	14	173	104	187
TBC30	1.90 ± 0.04	1 (fixed)	99.8 ± 0.8	2.61	30	205	104	235
TBC30	1.89 ± 0.06	0.99 ± 0.03	99.9 ± 0.9	2.82	30	205	104	235
TBCaNa	2.74 ± 0.06	1 (fixed)	99.4 ± 0.7	2.66	2.5	232	186	235
TBCaNa	2.72 ± 0.07	0.97 ± 0.03	99.7 ± 0.8	2.17	2.5	232	186	235

[a] Accompanying changes in [Cl^-], [Na^+], and total ionic strength I are also reported. [b] % rmsd is the percent weighted root-mean-square deviation between the predicted and experimental data.

Table 2: Kinetic Constants, Normalized to 1 NIH Unit of Thrombin/L, and Other Fitting Parameters (eq 4 with a β_b of 1 and eq 5) for the Release of FPB as a Function of Ca^{2+} Concentration[a]

buffer	K_b {$\times 10^5$ [(NIHu/L)s]$^{-1}$}	K_b' {$\times 10^5$ [(NIHu/L)s]$^{-1}$}	A	% rmsd[b]	[Ca^{2+}] (mM)	[Cl^-] (mM)	[Na^+] (mM)	I (mM)
TBE	1.75 ± 0.09	−	101.0 ± 2.1	13.2	0	145	106	150
TBE	1.79 ± 0.16	0.00 ± 0.08	101.0 ± 2.5	12.9	0	145	106	150
TBS	2.31 ± 0.14	−	98.5 ± 1.7	4.2	0	145	104	145
TBS	2.01 ± 0.21	0.25 ± 0.14	98.6 ± 1.7	7.8	0	145	104	145
TBC2.5	2.24 ± 0.12	−	100.0 ± 1.1	9.4	2.5	150	104	153
TBC2.5	2.13 ± 0.29	0.08 ± 0.18	100.0 ± 1.2	6.3	2.5	150	104	153
TBC14	1.71 ± 0.15	−	102.0 ± 3.1	16.3	14	173	104	187
TBC14	1.77 ± 0.34	0.00 ± 0.15	101.0 ± 3.6	17.5	14	173	104	187
TBC30	0.68 ± 0.07	−	99.4 ± 2.8	129.7	30	205	104	235
TBC30	0.54 ± 0.04	0.14 ± 0.03	101.0 ± 1.4	8.0	30	205	104	235
TBCaNa	1.24 ± 0.10	−	102.0 ± 3.0	59.1	2.5	232	186	235
TBCaNa	1.24 ± 0.19	0.00 ± 0.13	102.0 ± 3.5	59.0	2.5	232	186	235

[a] Accompanying changes in [Cl^-], [Na^+], and total ionic strength I are also reported. [b] % rmsd is the percent weighted root-mean-square deviation between the predicted and experimental data.

Their immunostained counterparts (lanes 2−4) fully reveal the degree of degradation, which was quantified by densitometric analysis conducted on lane 2, with the others being overloaded. To relate the level of degradation of our FG samples to that of circulating FG, we have also likewise analyzed blood samples obtained from two healthy donors. A representative analysis is shown in Figure 4B, which is a Y18-stained Western blot of a PAA gel where samples of plasma from a single donor (lanes 1−3) and of a purified FG (lane 4−6) from another source (Calbiochem, San Diego, CA) have been run side by side. The "overcrowding" effect clearly visible in lane 1 at the intact Aα-chain level is caused by the presence of serum albumin and other plasma proteins of similar molecular mass which were present in the plasma sample. From this comparison, one can note that the degradation at the C-terminal ends of the Aα-chains has a different pattern in the plasma and in the purified samples, the latter being more similar to our FG sample (panel A, lanes 2−4). Similar results were obtained with the other plasma sample (data not shown).

The results of the densitometric analysis for the FG sample in lane 2 of Figure 4A are shown in Figure 5. Using a Gaussian deconvolution procedure, up to 19 species were resolved in the profile, although some are very minor and could be just a deconvolution artifact (see Table 3, second column). To tentatively identify which proteolytic species were present, a calibration procedure was performed utilizing both the recombinant molecular mass standards and the undegraded FG chains. Since the amido black-stained nitrocellulose membrane shrunk somewhat on treatment (see Figure 4A), the relative migration factors R_f of the bands of the FG chains were normalized to those of the immunostained membrane, using the R_f of the recombinant protein standards in the two halves.

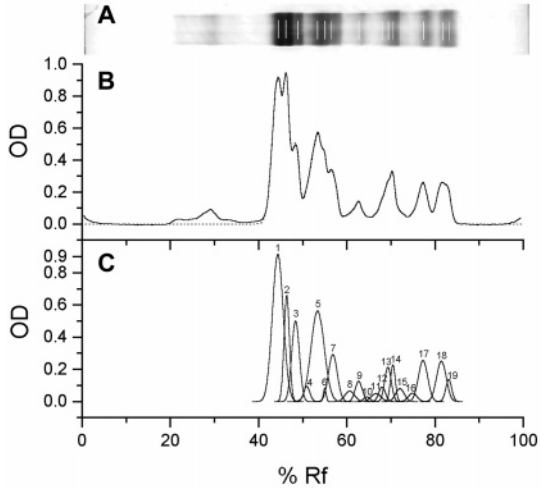

FIGURE 5: Deconvolution of the densitometric profile of lane 2 from Figure 4A. (A) Lane 2 of Figure 4A, where the thin vertical line marks the bands identified by the OneDScan software. (B) Original densitometric profile (solid line) superimposed with the sum of the Gaussians of panel C (dotted line). (C) Gaussians resulting from the deconvolution of the densitometric profile with the PeakFit software.

Table 3: Percent Areas, Molecular Masses from the SDS−PAGE/Western Blot Analysis, and Tentative Assignments to Known and Hypothetical Proteolytic Fragments, Based on the Calculated Molecular Masses, of Aα-Chain C-Terminal Fragments

fragment	% area	molecular mass from SDS−PAGE (Da)	molecular mass from sequence (Da)	residues	proteolytic site
$A\alpha_1$	24.83	65 445	66 253	1−610[a]	−
$A\alpha_2$	8.78	62 894	63 410	1−583[b]	K-M
$A\alpha_3$	9.35	60 443	60 180	(1−554?)	(R-G)
$A\alpha_4$	1.53	57 513	57 438	(1−528?)	(R-G)
$A\alpha_5$	18.18	54 725	55 193	1−508[b]	K-T
$A\alpha_6$	0.56	53 012	−	UD[d]	UD[d]
$A\alpha_7$	6.51	51 149	50 278	(1−461?)	(K-E)
$A\alpha_8$	1.61	47 334	48 908	(1−448?)	(K-T)
$A\alpha_9$	2.23	45 489	46 385	1−424[b]	R-T
$A\alpha_{10}$	0.48	43 891	−	UD[d]	UD[d]
$A\alpha_{11}$	1.27	42 097	−	UD[d]	UD[d]
$A\alpha_{12}$	1.53	40 941	−	UD[d]	UD[d]
$A\alpha_{13}$	3.52	39 897	−	UD[d]	UD[d]
$A\alpha_{14}$	2.74	39 034	−	UD[d]	UD[d]
$A\alpha_{15}$	1.73	37 812	−	UD[d]	UD[d]
$A\alpha_{16}$	1.16	35 694	34 468	1−309[c]	G-P
$A\alpha_{17}$	5.94	34 032	33 341	1−297[c]	G-G
$A\alpha_{18}$	5.96	31 368	30 851	1−269[c]	N-P
$A\alpha_{19}$	2.09	30 326	29 186	1−252[c]	R-G

[a] Full-length. [b] Known and putative (?) plasmin sites (*67*−*70*). [c] Cleavage points in plasma FG (*71*). [d] Undetermined.

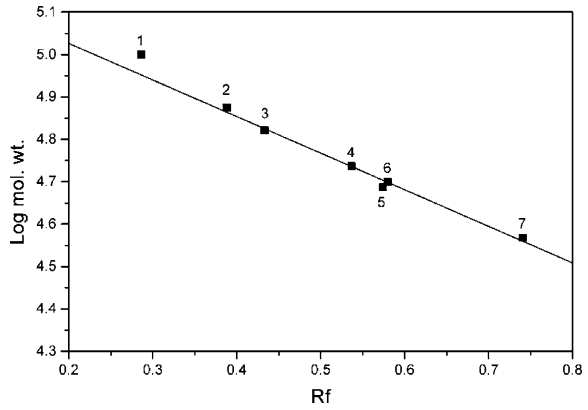

FIGURE 6: Molecular mass calibration curve for the gel of Figure 4. Data points 1, 2, 6, and 7 are the recombinant protein molecular mass standards (100 000, 75 000, 50 000, and 37 000 Da, respectively). Data points 3−5 are the FG Aα-, Bβ-, and γ-chains with molecular masses of 66 250, 54 480, and 48 650 Da, respectively.

The calibration curve is shown in Figure 6, where the two highest-molecular mass recombinant protein standards have not been taken into consideration (data not shown), being clearly outside of the linear range. Even so, when only the 100−37 kDa recombinant protein standards were used (points 1, 2, 6, and 7), the molecular masses of the FG chains were not recovered well. A better fit was obtained by excluding also the 100 kDa standard (point 1) and including the FG intact chains (points 3−5), as shown by the solid line in Figure 6. Therefore, the molecular masses of the bands of the FG Aα-chains were estimated using this line, and are reported in the third column of Table 3. A comparison with the molecular masses calculated from the FG Aα-chain sequence, using known (*67*−*70*) and potential plasmin and other reported (*71*) proteolytic sites, has allowed us to tentatively assign all the major bands to defined fragments, as reported in the three rightmost columns in Table 3. However, the identification of the relatively major $A\alpha_3$ and $A\alpha_7$ bands is only tentative, since the R554−G555 and K461−E462 plasmin sites have not been previously reported. In addition, six minor bands in the central region could not be assigned to known or potential sites. While our calibration procedure cannot guarantee the correct molecular mass determination especially in the lower range, it is also possible that these bands are the product of the digestion by other enzyme(s) (see ref *15*, and references therein). In any case, the identification of the major bands in the 45−70 kDa range appears to be reliable enough for our purposes.

To simplify the matters, we can tentatively assign the Aα-chain variant-containing FG subpopulations to two major groups. One possibility is to group the full-length chain and the first fragment together ($A\alpha_1$ and $A\alpha_2$ in Table 3, amounting to ∼34% of the population), since a recent report (*72*) has shown that residues Aα583−610 are likely to be unstructured, and group the remaining fragments as degraded. Alternatively, we can group together bands $A\alpha_1$−$A\alpha_4$ (∼45% of the total) and assume that important structural features are lost starting from the prominent $A\alpha_5$ band, which alone accounts for ∼18% of the total, grouping it with the more degraded species.

A similar analysis was performed on the plasma samples, for instance on that shown in lane 3 of Figure 4B, finding a somewhat different proportion in the $A\alpha_1$−$A\alpha_3$ fragments (47:31:20 in plasma vs 58:20:22 from the data in Table 3) (data not shown). Because of likely saturation effects, only an upper limit of degradation was estimated from lane 1 of Figure 4B, resulting in an ∼85:15 ratio between the $A\alpha_1$−$A\alpha_4$ and $A\alpha_5$−$A\alpha_{19}$ groups.

Another important source of polydispersity is in the C-terminal ends of the γ-chains, due to alternative splicing of the mRNA. The γ′-variant is particularly relevant for our study, since it is known to bind thrombin with high affinity at a nonsubstrate site (*73*−*75*). Using the MAbs 4A5, specific for normal γ-chains (*59*), and L2B, recognizing the γ′-variant only (*60*, *61*), the two forms were clearly identified on a Western blot after SDS−PAGE separation under reducing conditions on a 10% PAA gel (data not shown). Quantification of their relative amounts was then carried out on a third lane using MAb J88B, which recognizes both forms equally well, having its epitope in a sequence upstream of residue 400 of the γ-chains (*60*). As we have done for the Aα-chains, Gaussian deconvolution was employed to show that in our samples the γ′-form was ∼4.3% of the total, which is at the lower end of the reported spectrum (5−15%; see refs *74*−*77*, and references therein).

We can now calculate the free:γ′-bound thrombin ratio in our samples. To this end, we can use the stated activity of the thrombin lot (2330 NIH units/mg of protein, 1199 NIH units/mL), which leads to a nominal thrombin concentration of 0.51 mg/mL in our stock solution and of 5.32×10^{-5} mg/mL (1.5 nM) in our reaction mixtures. Alternatively, we can deduce the thrombin concentration in our stock solution from the kinetic titrations with the synthetic chromogenic substrate, which gave an initial velocity of 1.755×10^{-2} μmol/s for a 3717-fold enzyme dilution in the presence of 3352 μM substrate, at 25 °C. Using a K_M of 83 μM and a k_{cat} of 30 s^{-1} (*62*), the thrombin concentration of the stock solution was found to be some 6-fold lower, 2.23 μM, than that derived from the activity stated by the manufacturer and,

Table 4: Kinetic Constants, Normalized to 1 NIH Unit of Thrombin/L, and Other Fitting Parameters Obtained with eq 3 for the Release of FPA in TBC2.5 (I = 153 mM, $[Ca^{2+}]$ = 2.5 mM, $[Cl^-]$ = 150 mM, and $[Na^+]$ = 104 mM)

A_1 (fixed)	K_{a1} {$\times 10^5$ $[(NIHu/L)s]^{-1}$}	K_{a2} {$\times 10^5$ $[(NIHu/L)s]^{-1}$}	A_{tot}	% rmsd[a]	K_{a1}/K_{a2}
47.5[b]	9.38 ± 0.77	1.61 ± 0.17	99.1 ± 2.0	3.00	5.83
51.6[b]	8.60 ± 0.62	1.47 ± 0.18	99.4 ± 2.0	2.95	5.85
45	9.93 ± 0.89	1.69 ± 0.18	98.9 ± 1.9	3.05	5.86
55	8.06 ± 0.53	1.36 ± 0.18	99.6 ± 2.1	2.96	5.93
34	13.56 ± 2.20	2.08 ± 0.19	98.5 ± 2.0	3.53	6.51
66	6.69 ± 0.36	0.98 ± 0.19	100.0 ± 2.7	3.54	6.83
25	21.19 ± 9.97	2.51 ± 0.33	98.5 ± 2.7	4.35	8.44
75	5.79 ± 0.43	0.69 ± 0.51	100.0 ± 5.5	3.63	8.39

[a] % rmsd is the percent weighted root-mean-square deviation between the predicted and experimental data. [b] These values were fixed on the values found by the fitting routine when all the parameters were left free to float.

consequently, also in the reaction mixtures, ~0.23 nM. In any case, these differences do not change appreciably the free:bound thrombin ratio, which in this range is heavily dependent on the amount of γ'-chains. Using an association constant of 4.9 × 10^6 M^{-1} for the binding of thrombin to the γ'-chains (*73*), we can then estimate the free:γ'-bound thrombin ratio to be ~77:23.

Polydispersity and Kinetics in Buffer TBC2.5. With this information in hand, we fitted the FPA release data in TBC2.5 with a sum of two exponentials (eq 3), initially letting all the parameters float but imposing the constraint that $A_1 + A_2 = 100 \pm 1.5\%$. A good fit was obtained, with a k_{a1}/k_{a2} ratio of ~6 and relative amplitudes of ~48 and ~52% (curve not shown). Interestingly, the ratio between the amplitudes of the two exponentials in this fit is fairly close to the ratio of the percentage fractions of the α-chain C-terminal fragments obtained by grouping the $A\alpha_1-A\alpha_4$ and $A\alpha_5-A\alpha_{19}$ areas (45:55). Thus, since the fragment areas and the exponential amplitudes are both proportional to the concentration of the different species present in the sample, this result seems to suggest that the observed double-exponential kinetics may be attributed to FG polydispersity with the above-mentioned grouped fractions. Indeed, fixing one of the amplitudes to 45 or 55%, and letting the other vary, with the constraint that their sum be equal to 100 ± 1.5%, produced very similar results and very good fits, one of which is shown in Figure 3C (dashed and dotted line). Progressively worse fits were obtained when the Aα-chains 34:66 (not shown) or the free:γ'-bound thrombin 25:75 (dotted line) relative proportions were used as a constraint. However, it should be pointed out that all these fittings were somewhat sensitive to the initial guesses in the parameter's values, preventing us from finding true unique solutions for k_{a1} and k_{a2}.

The normalized K_{a1} and K_{a2} values that we have deduced from the two-exponential fitting of the data collected in TBC2.5 are then reported in Table 4. Compared with the single "average" K_a obtained with the stretched-exponential fit (Table 1), it is interesting to note that the double-exponential fit leads to a constant at least 2−3 times faster and another at least 2−3 times slower. Unfortunately, for the above-mentioned reasons, it was not possible to directly assign from the fittings the fast and slow constants to either of the groups within the tested sets (48:52, 45:55, 34:66, and 25:75). However, the very large values obtained for K_{a1}

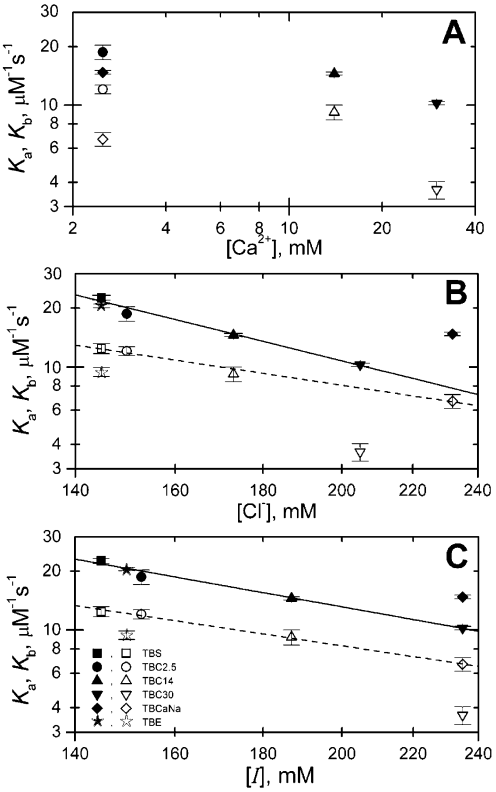

FIGURE 7: Log−log plots of the dependence of the K_a (filled symbols) and K_b (empty symbols; derived from the fittings with eq 4 where $\beta_b = 1$) values on Ca^{2+} concentration (A), Cl^- concentration (B), and I (C): (squares) TBS, (circles) TBC2.5, (up triangles) TBC14, (down triangles) TBC30, (diamonds) TBCaNa, and (stars) TBE. Superimposed in panels B and C are the results of linear regressions to the TBS, TBC14, and TBC30 data (FPA, solid lines) and to the TBS, TBC2.5, TBC14, and TBCaNa data (FPB, dashed lines).

when it was assigned to the minor component within the 34:64 and 25:75 groups can be taken as an indication that the faster constant could be associated with the major component. In any case, while within each set the K_{a1}/K_{a2} ratio is constant irrespective of the assignment, it increases from ~6 to ~8 on going from a ratio of 48:52 to 25:75.

Ionic Strength and Ca^{2+}-Specific Effects on FPA and FPB Release. In analogy to what Vindigni and Di Cera have done in their salt dependence study (*51*), we have plotted on log−log scales the K_a and K_b values versus either the Ca^{2+} concentration, the Cl^- concentration, or the total ionic strength I. To permit a comparison with the data of Vindigni and Di Cera (*51*), the K_a and K_b values listed in Tables 1, 2, and 4 were converted from units of $[(NIHu/L)s]^{-1}$ to M^{-1} s^{-1} using the thrombin concentration deduced from the titration with the synthetic substrate. As can be seen in Figure 7 [K_a (filled symbols) and K_b (empty symbols)], the Ca^{2+} concentration plots (panel A) did not show any defined linear dependence. Instead, linear dependencies were obtained for both constants versus either the Cl^- concentration (panel B) or I (panel C). The straight lines are derived from weighted linear regressions to the equations $\log(K) = A_0 + \Gamma_{[Cl^-]} \log[Cl^-]$ (panel B) and $\log(K) = A_0 + \Gamma_I \log(I)$ (panel C), and the resulting phenomenological parameters are reported in Table 5.

A first interesting observation is that the linear dependence on the Cl^- concentration or I of the K_a data (panels B and C, solid lines) was obtained at a constant Na^+ concentration

Table 5: Phenomenological Parameters Derived from the Linear Fits of the Plots in Panels B and C of Figure 7

	FPA		FPB	
	$[Cl^-]$	I	$[Cl^-]$	I
A_0	5.50 ± 0.1	6.02 ± 0.03	5.98 ± 0.07	5.99 ± 0.04
Γ	-2.18 ± 0.13	-1.58 ± 0.04	-1.33 ± 0.09	-1.33 ± 0.05
r^2	0.9962	0.9988	0.9900	0.9971

of 104 mM (TBS, TBC14, and TBC30 points included in the regression). In addition, the TBE value (filled stars) and even the "average" value obtained with the stretched-exponential fit in TBC2.5 (filled circles), obtained at 106 and 104 mM Na^+, respectively, are quite consistent with these linear dependencies. Moreover, our A_0 and Γ_I values derived from the K_a versus I plots (Table 5, third column) are strikingly similar to those obtained by Vindigni and Di Cera for their NaCl data (see Table 3 of ref *51*). Since in their case the NaCl concentration and I molarities practically coincide, this reinforces the idea of an electrostatic coupling between fibrinogen and thrombin which is nonspecifically screened by the different charged ions present in solution (*51*). The diverse A_0 and $\Gamma_{[Cl^-]}$ values obtained for the K_a versus Cl^- concentration plot simply reflect the contribution of the divalent Ca^{2+} cation to the ionic strength of the solutions. In other words, these data seem to imply that the FPA release by thrombin is affected mainly by the ionic strength of the solution. However, when the Na^+ concentration was increased in the presence of 2.5 mM $CaCl_2$ so as to reach the ionic strength of buffer TBC30, the points did not fall on the linear fits anymore (TBCaNa, filled diamonds, Figure 7B,C). Since Vindigni and Di Cera (*51*) obtained very similar A_0 and Γ_{salt} values for K_a as a function of the concentration of NaCl and NaF, this would suggest a Ca^{2+}-specific effect on FPA release, in contrast with the previous interpretation. One possibility is that this result derives from the particular combination of a physiological Ca^{2+} concentration, with its peculiar effects, and a higher than physiological I, suggesting a finely tuned mechanism for FPA release requiring optimal values of calcium and ionic strength. More experiments are clearly needed to better investigate this hypothesis.

Unexpectedly, an opposite effect was found for the K_b data (Figure 7B,C, empty symbols), where the points in TBCaNa (diamonds) lie on the same linear relations (dashed lines) with buffers TBS, TBC2.5, and TBC14 (squares, circles, and up triangles, respectively), while the points in TBC30 (down triangles) fall instead below them. At the same time, removal of the tightly bound Ca^{2+} ions (TBE, stars) also affected FPB release, seemingly in agreement with the dependence of the FPB cleavage on fibrin formation, whose rate is known to be enhanced by Ca^{2+} (see ref *2*, and references therein). Because of the exclusion of the high Ca^{2+} concentration point (TBC30) from the linear fit, practically identical A_0 and Γ values were obtained for the Cl^- concentration and I in this case (see Table 5, last two columns). However, contrary to the FPA case, our Γ values for FPB are nearly half of those reported by Vindigni and Di Cera (*51*) for the three salts they investigated, and much closer to our FPA values. As no free Ca^{2+} was added in their study, it is possible that the observed electrostatic screening effects are affected by its presence.

DISCUSSION

In this paper, we have reported some unexpected findings concerning the role of Ca^{2+} in the FP release by the physiological enzyme thrombin. This work was started to complement our light scattering studies on fibrin formation, which were carried out at 25 °C (*21*, *52*−*54*), and provides some additional evidence of the fine interplay between specific ion effects and the overall ionic strength of the solution in modulating the FP release. Moreover, there are strong hints that the C-terminal parts of the Aα-chains also are involved in this modulation. Although the polydispersity at the level of Aα-chains of circulating FG in healthy subjects is surely less, and seems to be restricted mainly to the higher-molecular mass species, it could still play a role in the kinetics of FP release. It is then interesting to try to put our findings on a broader perspective.

Comparing the Kinetic Parameters. To start, we can compare the data presented in Tables 1, 2, and 4 with the available literature data. Since we did not perform FG concentration dependence studies, we could not determine the Michaelis−Menten k_{cat} and K_M parameters. However, our FG concentration (0.5 mg/mL, ∼1.5 μM) was quite low, in any case well below the K_M literature values of 7−11 μM (*47*−*50*), while at the same time being much larger than the enzyme concentration (∼0.23−1.5 nM). Thus, our K_a and K_b values can be taken to be a close approximation to the specificity constants k_{cat}/K_M. Within this approximation, our K_a values are at the lower end of the available k_{cat}/K_M literature values (*47*−*50*), $\sim 4.8-11.2 \times 10^{-5}$ [(NIHu/L)s]$^{-1}$, which were, however, collected under different buffer conditions and using bovine and human fibrinogen and thrombin in various combinations. Clearly, these differences prevent a more detailed comparison between our K_a values and the literature k_{cat}/K_M values. Nevertheless, it is of interest to note that in none of the above-mentioned studies was the Ca^{2+} concentration increased above 1 mM, and thus the significant effect that we observed at 2.5 mM Ca^{2+} was likely not previously noticed. In any case, the values that we have obtained with the double-exponential fit for the 48:52 or 45:55 group are also fully compatible with the literature data.

To better visualize the differences induced by varying the Ca^{2+} concentration, in Figure 8 we have plotted a series of synthetic curves generated for the FPA and FPB release under all the conditions that were investigated using the normalized K_a and K_b values of Tables 1, 2, and 4. The significant effect of physiological Ca^{2+} concentration and I on the FPA release is quite apparent here (panel A, solid thick black curve), and it is evident that it derives from the sum of fast and slow K_a components represented by the solid gray curves. A further increase in the Ca^{2+} concentration to 14 mM [a concentration used, for instance, for *in vitro* thrombin activation of Factor XIII (*78*)] or to 30 mM [approaching the value of 50 mM used in the initial FG fragment D crystallization conditions (*5*)], however, completely abolished this effect, while progressively slowing the FPA release to about half its value under near-physiological conditions (Table 1 and Figure 8A).

With regard to the FPB release, first of all our data confirm the sequential mechanism supported by the work of Mihaly (*50*) and Vindigni and Di Cera (*51*), as shown by the good fittings to the data points of Figure 3. Only in TBC30 does

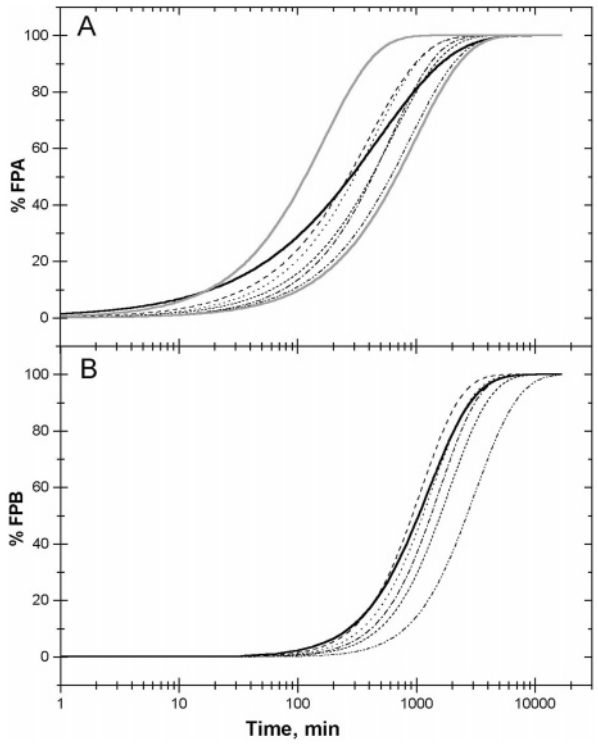

FIGURE 8: FPA and FPB synthetic release curves. The curves were generated from the data in Tables 1, 2, and 4 using eqs 2 and 3 (FPA, panel A) and eq 4 with a β_b of 1 (FPB, panel B): dotted lines for TBE, dashed lines for TBS, solid thick black lines (eq 2 with a β_a of 0.69, panel A; eq 4, panel B) and gray lines (eq 3 with a K_{a1} of 9.93×10^{-5} $[(\text{NIHu/L})\text{s}]^{-1}$ and a K_{a2} of 1.69×10^{-5} $[(\text{NIHu/L})\text{s}]^{-1}$, $A_1 = 45$, $A_2 = 55$) for TBC2.5, dashed and dotted lines for TBC14, dashed−dotted−dotted lines for TBC30, and short dashed lines for TBCaNa.

it appear that some FPB is released independent of prior FPA release, suggesting a Ca^{2+}-specific effect (see below). In addition, we note that, in contrast with what Mihaly (*50*) found, our specificity constants (K_a and K_b) are not the same for FPA and FPB, but rather, their ratio is roughly 0.5 for any given buffer. More importantly, the strong, population-dependent effect on the FPA release observed with buffer TBC2.5 is not carried out to the FPB release, further supporting the concept of a sequential mechanism. The slight crossover exhibited by the FPB synthetic release curve (thick black curve in Figure 8B) is only a consequence of the FPA kinetics under these conditions.

Polydispersity and Ca^{2+}. The fact that the FPA data in TBC2.5 are fitted equally well by the double-exponential (eq 3) and stretched-exponential (eq 2) decay functions suggests that is reasonable to associate the stretched-exponential decay behavior with sample polydispersity, rather than with time-dependent rate constants (see refs *65* and *66*). Thus, it is possible to interpret the stretch exponent β_a as a parameter which reflects the substrate polydispersity (*65*). From the results of the double-exponential fittings (Table 4) and the polydispersity analysis, the noticeable and opposite effects of physiological Ca^{2+} concentration and *I* on two FG subpopulations seem to suggest the involvement of the C-terminal parts of the Aα-chains, thus reinforcing the hypothesis that they may play an important role in the early events in fibrin polymerization (*13*, *79*). But why is this effect noticeable only at a physiological Ca^{2+} concentration and *I*? Most likely, it involves a Ca^{2+}-binding site being present in one subpopulation only, but it is not clear if this should be a high- or low-affinity site. Its disappearance at Ca^{2+} concentrations higher than physiological could suggest a saturation effect more compatible with a low-affinity site. On the other hand, the effect disappears with an increase in *I* with NaCl, while the Ca^{2+} concentration is kept at a physiological value. This makes it more likely that a high-affinity Ca^{2+}-binding site is instead involved, but modulated by *I*, which, under our conditions, increases as the Ca^{2+} concentration increases.

In any case, where is this site located? As pointed out in the introductory section, there is still some uncertainty about the precise number, class, and localization of Ca^{2+}-binding sites in FG. For instance, a reanalysis of earlier data by Nieuwenhuizen, Haverkate, and colleagues (*34*) seemed to indicate that, in contrast with rat FG that has 2.4 high-affinity binding sites and 2.3 lower-affinity sites, human FG has just 3 high-affinity sites under near-physiological conditions [50 mM Tris and 150 mM NaCl (pH 7.5)]. However, our own reanalysis of the data presented in Figure 1 of Nieuwenhuizen et al. (*33*) for human FG, using eq 1 of ref *34* inserted in the TableCurve 2D curve fitting program (version 4.07, SPSS, Systat Software Inc.), has indicated that an equally good fit can be obtained with 2.2 ± 0.8 high-affinity [$K_d = (11 \pm 5) \times 10^{-6}$ M] and ∼14 low-affinity ($K_d \sim 2 \times 10^{-3}$ M) sites. Interestingly, Marguerie et al. (*36*) earlier reported 3 high-affinity and 14 low-affinity sites (2.56 ± 0.6 and ∼16, respectively, in our reanalysis of their Figure 2 data) for bovine FG in 5 mM Tris and 0.5 M NaCl (pH 7.5), which were however reduced to just 2 high-affinity sites when the pH was reduced to 6.0. Furthermore, they subsequently showed (*42*) that the third pH-dependent site was present in human FG ($K_d \sim 9 \times 10^{-6}$ M) only when the Aα-chains were intact, suggesting that it could be, for symmetry reasons, a composite site involving the two halves of the molecule. In addition, no Ca^{2+} ions were found in the recently published FG central E domain structure (*80*), although it lacked residues Aα1−28 and Bβ1−60. In the end, a consensus exists only for the two high-affinity Ca^{2+}-binding sites, which were clearly localized in the FG outer D domains (*5*−*8*), confirming previous biochemical work (see ref *35*, and references therein). The odd number of high-affinity sites may result from the inherent heterogeneity of the FG population, but the above-mentioned study by Marguerie (*42*) makes it an unlikely possibility. Rather, it is the noninteger number of sites recalculated by us from the data of Nieuwenhuizen et al. (*33*) and Marguerie et al. (*36*) that simply suggests heterogeneity in their FG samples. It should also be mentioned that the γ′-chain isoform likely harbors a Ca^{2+}-binding site (*81*), but in any case, its relatively small amounts [5−15% (*74*−*77*), ∼4.3% in our samples] cannot fully account for the third high-affinity site.

As for the Ca^{2+} low-affinity sites, the recently identified new sites in the D domain (*37*−*39*) probably belong to this class, and one of them could well be the site of Ca^{2+} uptake shown by Mihaly (*46*) to occur after FPB release, as already suggested (*38*). Therefore, they are more likely to be involved in the lateral aggregation of fibrin fibers, and perhaps in FPB cleavage, although their position with respect to the central E domain will call for a long-distance propagation of a conformational change (see more below). Sialic acid residues, which are located at the end of the two carbohydrate clusters

present in each half of FG, have also been implicated in Ca^{2+} binding and shown to modulate the lateral aggregation of the fibers (*40*). While one carbohydrate cluster is present in the D domain (attached to Asnβ364), and thus unlikely to directly influence the FP cleavage, the other is attached to Asnγ52, reasonably close to the central E domain. Thus, it is potentially involved either in thrombin binding or in interactions with the C-terminal ends of the Aα-chains. It is difficult to envisage a specific role for the other, not yet identified, low-affinity sites.

An aid in resolving this puzzle may come from the electron microscopy works of Veklich et al. (*13*) and Gorkun et al. (*79*), who studied the effect of pH and of FP removal on the fourth domain presumably formed by the C-terminal parts of the Aα-chains and positioned on top of the E domain. To start, this domain is completely absent in the so-called "fragment X" preparations, lacking part or most of the C-terminal parts of the Aα-chains. Moreover, consistent with the loss of the putative third high-affinity Ca^{2+}-binding site with a reduction in pH (*36*), at pH 3.5 the fourth domain was separated into two smaller domains positioned away from the E domain in both fibrinogen and fibrin (*13*). Interestingly, when the samples were observed at pH 7.4 and in the presence of Ca^{2+}, removal of the FPAs alone induced only a detachment of the fourth domain from the E domain in ~15% of the molecules, this number becoming 71% if both sets of FPs are cleaved (*13*, *79*). Thus, this domain appears to be made primarily by the C-terminal parts of the Aα-chains, and to require the presence of the FPs only to hold it closer to the central E domain. It is also possible that the repositioning of the fourth domain is just a consequence of conformational changes induced by the removal of the FPs.

In the end, it seems therefore more likely that the putative composite high-affinity Ca^{2+}-binding site involves the C-terminal parts of the Aα-chains, held together over the central E domain where the negatively charged fibrinopeptides are located. According to this picture, this site could be lost following the partial degradation of the C-terminal parts of the Aα-chains, possibly leading to a change first in FPA availability. Whether this effect will produce an increase or a decrease in the efficiency of FPA cleavage is difficult to asses from our data, and will require further studies involving purified FG fractions differing in the degradation of the C-terminal parts of the Aα-chains. Additional controls on the role of the γ'-chain isoform will be likewise required, although a very recent report (*82*) has shown that FPB, and not FPA release, is affected (slowed), at least under the one particular condition that was investigated (50 mM Tris, 100 mM NaCl, 10 mM $CaCl_2$, pH 7.5, with $I = 175$ mM).

Ionic Strength and Ca^{2+}-Specific Effects. Besides the polydispersity effects, it is also interesting to further discuss the specific effects of Ca^{2+} concentration and *I* on FP release. Taken together, the data in Figure 7 show that while the cleavage rates of both FPA and FPB depend in a similar manner on the ionic strength of the solution, they respond differently to the presence of Ca^{2+}. While a specific effect on FPA release is observed only at a physiological Ca^{2+}-concentration and *I*, removal of the Ca^{2+} ions tightly bound to FG by EDTA (TBE) slows FPB cleavage; however, a Ca^{2+} concentration well above the physiological level also inhibits FPB release by more than it would be expected from purely screening effects. We also note that this high Ca^{2+} concentration at the same time allows some FPB to be cleaved independent of prior FPA release (see Figure 3E and Table 2). This is interesting in light of the elegant work by Mullin et al. (*83*) with recombinant fibrinogens, showing that the order of FP release is dictated by thrombin specificity. In particular, it was proposed that a conformational change in either thrombin or FG (or both) occurs after FPA release, allowing the subsequent efficient cleavage of FPB. It is possible that such a conformational change may be initiated at these rather high Ca^{2+} concentrations, suggesting the involvement of a low-affinity Ca^{2+}-binding site. It is tempting to speculate that this may be one of the recently discovered (*37*−*39*) additional Ca^{2+}-binding sites in the D domain, as already mentioned in the previous section. In fact, one of these sites (*37*) has been observed in a D dimer fragment after the engagement of a synthetic *B* knob-like peptide in the *b* hole, leading to a rearrangement of the β-subdomain in a way that favors the lateral aggregation of the fibrin fibers (*19*, *37*). Perhaps, at our relatively high (30 mM) Ca^{2+} concentration the site becomes occupied, inducing a conformation change even without the *B* knob engagement. Thus, one wonders if this conformational change can somewhat propagate back along the coiled coil to the central domain, directly influencing FPB cleavage. It should be also mentioned that while two of the additional Ca^{2+}-binding sites have been also observed in a recombinant human non-cross-linked fragment D free of ligands, in the presence of both synthetic *A* and *B* knobs the above-mentioned site is surprisingly lost (*39*). Although this effect may be due to the concentration of free Ca^{2+} in the crystallizing solutions being much higher in the absence than in the presence of the synthetic knobs (70 vs 12.5 mM) (*39*), a conformational change caused by the absence of the D−D dimer interface cannot be ruled out. Further studies on the FP release while FG polymerization is inhibited by an excess of either small peptides or fragment D should help to clarify this matter.

NOTE ADDED AFTER ASAP POSTING

In the version of this paper published 09/30/03, the Γ in the first column of Table 5 appeared incorrectly as *G*. The correct version was published 09/30/03.

ACKNOWLEDGMENT

We thank R. Cancedda for support, F. Tosetti for help, R. F. Doolittle for help and advice, and E. Di Cera for very useful discussions and suggestions. Thanks are also due to Mike Mosesson and to two anonymous reviewers for their critiques, for suggesting alternative hypotheses, and for pointing out to us some key references.

REFERENCES

1. Doolittle, R. F. (2000) The molecular basis of fibrin, in *The Molecular Basis of Blood Diseases* (Stamatoyannopoulos, G., Majerus, P. W., Perlmutter, R. M., and Varmus, H., Eds.) 3rd ed., pp 719−739, Saunders, Philadelphia.
2. Blomback, B. (1996) Fibrinogen and fibrin: proteins with complex roles in hemostasis and thrombosis, *Thromb. Res. 83*, 1−75.
3. Doolittle, R. F. (1984) Fibrinogen and fibrin, *Annu. Rev. Biochem. 53*, 195−229.
4. Mosesson, M. W., and Doolittle, R. F., Eds. (1983) *Molecular Biology of Fibrinogen and Fibrin*, Annals of the New York Academy of Sciences Vol. 406, New York Academy of Sciences, New York.

5. Yee, V. C., Pratt, K. P., Cote, H. C. F., Letrong, I., Chung, D. W., Davie, E. W., Stenkamp, R. E., and Teller, D. C. (1997) Crystal structure of a 30 kDa C-terminal fragment from the γ-chain of human fibrinogen, *Structure 5*, 125−138.
6. Spraggon, G., Everse, S. J., and Doolittle, R. F. (1997) Crystal structures of fragment D from human fibrinogen and its crosslinked counterpart from fibrin, *Nature 389*, 455−462.
7. Brown, J. H., Volkmann, N., Henschen-Edman, A. H., and Cohen, C. (2000) The crystal structure of modified bovine fibrinogen, *Proc. Natl. Acad. Sci. U.S.A. 97*, 85−90.
8. Yang, Z., Kollman, J. M., Pandi, L., and Doolittle, R. F. (2001) Crystal structure of native chicken fibrinogen at 2.7 Å resolution, *Biochemistry 40*, 12515−12523.
9. Mosesson, M. W., Hainfeld, J., Wall, J., and Haschemeyer, R. H. (1981) Identification and mass analysis of human fibrinogen molecules and their domains by scanning transmission electron microscopy, *J. Mol. Biol. 153*, 695−718.
10. Medved′, L. V., Gorkun, O. V., and Privalov, P. L. (1983) Structural organization of C-terminal parts of fibrinogen Aα-chains, *FEBS Lett. 160*, 291−295.
11. Erickson, H. P., and Fowler, W. E. (1983) Electron microscopy of fibrinogen, its plasmic fragments and small polymers, in *Molecular Biology of Fibrinogen and Fibrin* (Mosesson, M. W., and Doolittle, R. F., Eds.) Annals of the New York Academy of Sciences Vol. 406, pp 146−163, New York Academy of Sciences, New York.
12. Weisel, J. W., Stauffacher, C. V., Bullit, T. E., and Cohen, C. (1985) A model for fibrinogen: domains and sequence, *Science 230*, 1388−1391.
13. Veklich, Y. I., Gorkun, O. V., Medved, L. V., Nieuwenhuizen, W., and Weisel, J. W. (1993) Carboxyl-terminal portions of the α chains of fibrinogen and fibrin. Localization by electron microscopy and the effects of isolated αC fragments on polymerization, *J. Biol. Chem. 268*, 13577−13585.
14. Mosesson, M. W. (1983) Fibrinogen heterogeneity, in *Molecular Biology of Fibrinogen and Fibrin* (Mosesson, M. W., and Doolittle, R. F., Eds.) Annals of the New York Academy of Sciences Vol. 406, pp 97−113, New York Academy of Sciences, New York.
15. Henschen-Edman, A. (2001) Fibrinogen non-inherited heterogeneity and its relationship to function in health and disease, in *Fibrinogen. XVIth International Fibrinogen Workshop* (Nieuwenhuizen, W., Mosesson, M. W., and De Maat, P. M., Eds.) Annals of the New York Academy of Sciences Vol. 936, pp 580−593, New York Academy of Sciences, New York.
16. Di Cera, E., Dang, Q. D., and Ayala, Y. M. (1997) Molecular mechanisms of thrombin function, *Cell. Mol. Life Sci. 53*, 701−730.
17. Hurlet-Jensen, A., Cummins, H. Z., Nossel, H. L., and Liu, C. Y. (1982) Fibrin polymerization and release of fibrinopeptide B by thrombin, *Thromb. Res. 27*, 419−427.
18. Weisel, J. W. (1986) Fibrin assembly. Lateral aggregation and the role of the two pairs of fibrinopeptides, *Biophys. J. 50*, 1079−1093.
19. Yang, Z., Mochalkin, I., and Doolittle, R. F. (2000) A model of fibrin formation based on crystal structures of fibrinogen and fibrin fragments complexed with synthetic peptides, *Proc. Natl. Acad. Sci. U.S.A. 97*, 14156−14161.
20. Janmey, P. A. (1982) Kinetics of formation of fibrin oligomers. I. Theory, *Biopolymers 21*, 2253−2264.
21. Bernocco, S., Ferri, F., Profumo, A., Cuniberti, C., and Rocco, M. (2000) Polymerization of rod-like macromolecular monomers studied by stopped-flow, multi-angle light scattering: set-up, data processing, and application to fibrin formation, *Biophys. J. 79*, 561−583.
22. Shainoff, J. R., Smejkal, G. B., DiBello, P. M., Mitkevich, O. V., Levy, P. J., Dempfle, C. E., and Lill, H. (1996) Isolation and characterization of the fibrin intermediate arising from cleavage of one fibrinopeptide A from fibrinogen, *J. Biol. Chem. 271*, 24129−24137.
23. Shainoff, J. R., Smejkal, G. B., DiBello, P. M., Sung, S. S., Bush, L. A., and Di Cera, E. (2002) Allosteric effects potentiating the release of the second fibrinopeptide A from fibrinogen by thrombin, *J. Biol. Chem. 277*, 19367−19373.
24. Li, X., Galanakis, D., and Gabriel, D. A. (1996) Transient intermediates in the thrombin activation of fibrinogen: Evidence for only the desAA species, *J. Biol. Chem. 271*, 11767−11771.
25. Meh, D. A., Siebenlist, K. R., Bergtrom, G., and Mosesson, M. W. (1995) Sequence of release of fibrinopeptide A from fibrinogen molecules by thrombin or Atroxin, *J. Lab. Clin. Med. 125*, 384−391.
26. Shainoff, J. R., Ratnoff, O. D., Smejkal, G. B., DiBello, P. M., Welches, W. R., Lill, H., Mitkevich, O. V., and Periman, P. (2001) Confirmation of Mendelian properties of heterodimeric fibrinogen molecules in a heterozygotic dysfibrinogenemia, "fibrinogen Amarillo", using GPRphoresis to differentiate semifibrin molecules from fibrinogen and fibrin, *Thromb. Res. 101*, 91−99.
27. Costantini, V., and Zacharski, L. R. (1992) The role of fibrin in tumor metastasis, *Cancer Metastasis Rev. 11*, 283−290.
28. Nagy, J. A., Brown, L. F., Senger, D. R., Lanir, N., Van De Water, L., Dvorak, A. M., and Dvorak, H. F. (1988) Pathogenesis of tumor stroma generation: a critical role for leaky blood vessels and fibrin deposition, *Biochim. Biophys. Acta 948*, 305−326.
29. Rickles, F. R., Levine, M., and Edwards, R. L. (1992) Hemostatic alterations in cancer patients, *Cancer Metastasis Rev. 11*, 237−248.
30. Milroy, R., Douglas, J. T., Campbell, J., Carter, R., Lowe, G. D., and Banham, S. W. (1988) Abnormal haemostasis in small cell lung cancer, *Thorax 43*, 978−981.
31. Korte, W. (2000) Changes of the coagulation and fibrinolysis system in malignancy: their possible impact on future diagnostic and therapeutic procedures, *Clin. Chem. Lab. Med. 38*, 679−692.
32. van Ruijven-Vermeer, I. A. M., Nieuwenhuizen, W., and Nooijen, W. J. (1978) Ca binding of rat fibrinogen and fibrin(ogen) degradation products, *FEBS Lett. 93*, 177−180.
33. Nieuwenhuizen, W., Vermond, A., Nooijen, W. J., and Haverkate, F. (1979) Calcium-binding properties of human fibrin(ogen) and degradation products, *FEBS Lett. 98*, 257−259.
34. Nieuwenhuizen, W., van Ruijven-Vermeer, I. A. M., Nooijen, W. J., Vermond, A., Haverkate, F., and Hermans, J. (1981) Recalculation of calcium-binding properties of human and rat fibrin(ogen) and their degradation products, *Thromb. Res. 22*, 653−657.
35. Nieuwenhuizen, W., and Haverkate, F. (1983) Calcium-binding regions in fibrinogen, in *Molecular Biology of Fibrinogen and Fibrin* (Mosesson, M. W., and Doolittle, R. F., Eds.) Annals of the New York Academy of Sciences Vol. 406, pp 92−96, New York Academy of Sciences, New York.
36. Marguerie, G., Chagniel, G., and Suscillon, M. (1977) The binding of calcium to bovine fibrinogen, *Biochim. Biophys. Acta 490*, 94−103.
37. Everse, S. J., Spraggon, G., Veerapandian, L., Riley, M., and Doolittle, R. D. (1998) Crystal structure of fragment double-D from human fibrin with two different bound ligands, *Biochemistry 37*, 8637−8642.
38. Everse, S. J., Spraggon, G., Veerapandian, L., and Doolittle, R. D. (1999) Conformational changes in fragments D and double-D from human fibrin(ogen) upon binding the peptide ligand Gly-His-Arg-Pro-amide, *Biochemistry 38*, 2941−2946.
39. Kostelansky, M. S., Betts, L., Gorkun, O. V., and Lord, S. T. (2002) 2.8 Å crystal structures of recombinant fibrinogen fragment D with and without two peptide ligands: GHRP binding to the "b" site disrupts its nearby calcium-binding site, *Biochemistry 41*, 12124−12132.
40. Dang, C. V., Shin, C. K., Bell, W. R., Nagaswami, C., and Weisel, J. W. (1989) Fibrinogen sialic acid residues are low affinity calcium-binding sites that influence fibrin assembly, *J. Biol. Chem. 264*, 15104−15108.
41. Marguerie, G. (1977) The binding of calcium to fibrinogen: some structural features, *Biochim. Biophys. Acta 494*, 172−181.
42. Marguerie, G., and Ardaillou, N. (1982) Potential role of the Aα chain in the binding of calcium to human fibrinogen, *Biochim. Biophys. Acta 701*, 410−412.
43. Haverkate, F., and Timan, G. (1977) Protective effect of calcium in the plasmin degradation of fibrinogen and fibrin fragments D, *Thromb. Res. 10*, 803−812.
44. Shen, L. L., McDonagh, R. P., McDonagh, J., and Hermans, J., Jr. (1974) Fibrin gel structure: influence of calcium and covalent cross-linking on the elasticity, *Biochem. Biophys. Res. Commun. 56*, 793−798.
45. Okada, M., and Blomback, B. (1983) Calcium and fibrin gel structure, *Thromb. Res. 29*, 269−280.
46. Mihalyi, E. (1988) Clotting of bovine fibrinogen. Calcium binding to fibrin during clotting and its dependence on release of fibrinopeptide B, *Biochemistry 27*, 967−976.

47. Martinelli, R. A., and Scheraga, H. A. (1980) Steady-state kinetic study of bovine thrombin-fibrinogen interaction, *Biochemistry 19*, 2343−2350.
48. Higgins, D. L., Lewis, S. D., and Shafer, J. A. (1983) Steady-state kinetic parameters for the thrombin-catalyzed conversion of human fibrinogen to fibrin, *J. Biol. Chem. 258*, 9276−9282.
49. Hanna, L. S., Scheraga, H. A., Francis, C. W., and Marder, V. J. (1984) Comparison of structures of various human fibrinogens and a derivative thereof by a study of the kinetics of release of fibrinopeptides, *Biochemistry 23*, 4681−4687.
50. Mihalyi, E. (1988) Clotting of bovine fibrinogen. Kinetic analysis of the release of fibrinopeptides by thrombin and of the calcium uptake upon clotting at high fibrinogen concentrations, *Biochemistry 27*, 976−982.
51. Vindigni, A., and Di Cera, E. (1996) Release of fibrinopeptides by the slow and fast forms of thrombin, *Biochemistry 35*, 4417−4426.
52. Rocco, M., Bernocco, S., Turci, M., Profumo, A., Cuniberti, C., and Ferri, F. (2001) Early events in the polymerization of fibrin, in *Fibrinogen. XVIth International Fibrinogen Workshop* (Nieuwenhuizen, W., Mosesson, M. W., and De Maat, P. M., Eds.) Annals of the New York Academy of Sciences Vol. 936, pp 167−185, New York Academy of Sciences, New York.
53. Ferri, F., Greco, M., Arcòvito, G., Andreasi Bassi, F., De Spirito, M., Paganini, E., and Rocco, M. (2001) Growth kinetics and structure of fibrin gels, *Phys. Rev. E 63*, 031401-1/17.
54. Ferri, F., Greco, M., Arcòvito, G., De Spirito, M., and Rocco, M. (2002) Structure of fibrin gels studied by elastic light scattering techniques: dependence of fractal dimension, gel crossover length, fiber diameter and fiber density on monomer concentration, *Phys. Rev. E 66*, 011913-1/13.
55. Mihalyi, M. (1968) Physicochemical studies of bovine fibrinogen. IV. Ultraviolet absorption and its relation to the structure of the molecule, *Biochemistry 7*, 208−223.
56. Laemmli, U. K. (1970) Cleavage of structural proteins during the assembly of the head of bacteriophage T4, *Nature 227*, 680−685.
57. Koppert, P. W., Huijsmans, C. M. G., and Nieuwenhuizen, W. (1985) A monoclonal antibody, specific for human fibrinogen, fibrinopeptide A-containing fragments and not reacting with free fibrinopeptide A, *Blood 66*, 503−507.
58. Fornace, A. J., Jr., Cummings, D. E., Comeau, C. M., Kant, J. A., and Crabtree, G. R. (1984) Structure of the human γ-fibrinogen gene. Alternate mRNA splicing near the 3′ end of the gene produces γA and γB forms of γ-fibrinogen, *J. Biol. Chem. 259*, 12826−12830.
59. Shiba, E., Lindon, J. N., Kushner, L., Matsueda, G. R., Hawiger, J., Kloczewiak, M., Kudryk, B., and Salzman, E. W. (1991) Antibody-detectable changes in fibrinogen adsorption affecting platelet activation on polymer surfaces, *Am. J. Physiol. 260*, C965−C974.
60. Haidaris, P. J., Francis, C. W., Sporn, L. A., Arvan, D. S., Collichio, F. A., and Marder, V. J. (1989) Megakaryocyte and hepatocyte origins of human fibrinogen biosynthesis exhibit hepatocyte-specific expression of γ chain-variant polypeptides, *Blood 74*, 743−750.
61. Haidaris, P. J., Peerschke, E. I. B., Marder, V. J., and Francis, C. W. (1989) The C-terminal sequences of the γ57.5 chain of human fibrinogen constitute a plasmin sensitive epitope that is exposed in crosslinked fibrin, *Blood 74*, 2437−2444.
62. Lottenberg, R., Christensen, U., Jackson, C. M., and Coleman, P. L. (1981) Assay of coagulation proteases using peptide chromogenic and fluorogenic substrates, *Methods Enzymol. 80*, 341−361.
63. Kehl, M., Lottspeich, F., and Henschen, A. (1981) Analysis of human fibrinopeptides by high-performance liquid chromatography, *Hoppe-Seyler's Z. Physiol. Chem. 362*, 1661−1664.
64. Bevington, P. R. (1991) *Data reduction and error analysis for the physical sciences*, McGraw-Hill, New York.
65. Pratap, P. R., Hellen, E. H., Palit, A., and Robinson, J. D. (1997) Transient kinetics of substrate binding to Na^+/K^+-ATPase measured by fluorescent quenching, *Biophys. Chem. 69*, 137−151.
66. Metzler, R., Klafter, J., Jortner, J., and Volk, M. (1998) Multiple time scales for dispersive kinetics in early events of peptide folding, *Chem. Phys. Lett. 293*, 477−484.
67. Takagi, T., and Doolittle, R. F. (1975) Amino acid sequence studies on the α-chain of human fibrinogen. Location of four plasmin attack points and a covalent cross-linking site, *Biochemistry 14*, 5149−5155.
68. Cottrell, B. A., and Doolittle, R. F. (1976) The amino acid sequence of a 27-residue peptide released from the α-chain carboxy-terminus during the plasmic digestion of human fibrinogen, *Biochem. Biophys. Res. Commun. 71*, 754−761.
69. Strong, D. D., Watt, K. W., Cottrell, B. A., and Doolittle, R. F. (1979) Amino acid sequence studies on the α-chain of human fibrinogen. Complete sequence of the largest cyanogen bromide fragment, *Biochemistry 18*, 5399−5404.
70. Watt, K. W., Cottrell, B. A., Strong, D. D., and Doolittle, R. F. (1979) Amino acid sequence studies on the α-chain of human fibrinogen. Overlapping sequences providing the complete sequence, *Biochemistry 18*, 5410−5416.
71. Nakashima, A., Sasaki, S., Miyazaki, K., Miyata, T., and Iwanaga, S. (1992) Human fibrinogen heterogeneity: the COOH-terminal residues of defective Aα chains of fibrinogen II, *Blood Coagulation Fibrinolysis 3*, 361−370.
72. Tsurupa, G., Tsonev, L., and Medved, L. (2002) Structural organization of the fibrin(ogen) αC-domain, *Biochemistry 41*, 6449−6459.
73. Meh, D. A., Siebenlist, K. R., and Mosesson, M. W. (1996) Identification and characterization of the thrombin binding sites on fibrin, *J. Biol. Chem. 271*, 23121−23125.
74. Meh, D. A., Mosesson, M. W., Siebenlist, K. R., Simpson-Haidaris, P. J., Brennan, S. O., DiOrio, J. P., Thompson, K., and Di Minno, G. (2001) Fibrinogen Naples I (Bβ A68T) nonsubstrate thrombin-binding capacities, *Thromb. Res. 103*, 63−73.
75. Meh, D. A., Siebenlist, K. R., Brennan, S. O., Holyst, T., and Mosesson, M. W. (2001) The amino acid sequence in fibrin responsible for high affinity thrombin binding, *Thromb. Haemostasis 85*, 470−474.
76. Moaddell, M., Falls, L. A., and Farrell, D. H. (2000) The role of γA/γ' fibrinogen in plasma factor XIII activation, *J. Biol. Chem. 275*, 32135−32140.
77. Lovely, R. S., Falls, L. A., Al-Mondhiry, H. A., Chambers, C. E., Sexton, G. J., Ni, H., and Farrell, D. H. (2002) Association of γA/γ' fibrinogen levels and coronary artery disease, *Thromb. Haemostasis 88*, 26−31.
78. Hornyak, T. J., Bishop, P. D., and Shafer, J. A. (1989) α-Thrombin-catalyzed activation of human platelet Factor XIII: relationship between proteolysis and Factor XIIIa activity, *Biochemistry 28*, 7326−7332.
79. Gorkun, O. V., Veklich, Y. I., Medved′, L. V., Henshen, A. H., and Weisel, J. W. (1994) Role of the αC domains of fibrin in clot formation, *Biochemistry 33*, 6986−6997.
80. Madrazo, J., Brown, J. H., Litvinovich, S., Dominguez, R., Yakovlev, S., Medved, L., and Cohen, C. (2001) Crystal structure of the central region of bovine fibrinogen (E5 fragment) at 1.4-Å resolution, *Proc. Natl. Acad. Sci. U.S.A. 98*, 11967−11972.
81. Moaddel, M., Farrell, D. H., Daugherty, M. A., and Fried, M. G. (2000) Interactions of human fibrinogens with factor XIII: Roles of calcium and the γ' peptide, *Biochemistry 39*, 6698−6705.
82. Cooper, A. V., Standeven, K. F., and Ariens, R. A. S. (2003) Fibrinogen γ-chain splice variant γ' alters fibrin formation and structure, *Blood 102*, 535−540.
83. Mullin, J. L., Gorkun, O. V., Binnie, C. G., and Lord, S. T. (2000) Recombinant fibrinogen studies reveal that thrombin specificity dictates order of fibrinopeptide release, *J. Biol. Chem. 275*, 25239−25246.

BI034411E